A Preliminary Examination of Warm Season Precipitation Displacement Errors in the Upper Midwest in the HRRRE and HREF Ensembles

BENJAMIN M. KIEL,[a] WILLIAM A. GALLUS, JR.,[a] KRISTIE J. FRANZ,[a] AND NATHAN ERICKSON[a]

[a] *Department of Geological and Atmospheric Sciences, Iowa State University, Ames, Iowa*

(Manuscript received 10 April 2021, in final form 4 March 2022)

ABSTRACT: Increased operational use of convection-allowing models and ensembles offers substantial improvements for some aspects of convective weather forecasting; however, errors in quantitative precipitation forecasts (QPFs) from these models, especially those related to incorrect placement of heavy rainfall systems, limit their usefulness as an input into hydrological models. To improve understanding of QPF location errors, this study quantifies the displacement errors for the centroids of both 0–18-h accumulated rainfall and rainfall in the first hour after initiation of precipitation systems in both the High-Resolution Rapid Refresh Ensemble (HRRRE) and the High-Resolution Ensemble Forecast (HREF) for 30 events in the 2018 warm season. Ensemble member QPFs are compared to quantitative precipitation estimates (QPEs) obtained from the North Central River Forecast Center (NCRFC). HRRRE is found to have less spread in centroid locations than HREF, and both HRRRE and HREF 0–18-h QPF accumulations have less spread than the 1-h QPF accumulation when the precipitation event initiates. Furthermore, QPF centroids are most often displaced to the west in HRRRE for both 0–18-h QPF accumulation and the 1-h QPF accumulation when the precipitation event initiates. The 0–18-h QPF accumulation displacement errors can be reduced when adjustments are made to the forecasted position based upon displacement errors present in the first hour of precipitation, but only when the adjustments are a function of the intercardinal quadrant in which the initial hour QPF centroid was displaced.

KEYWORDS: North America; Ensembles; Forecasting; Short-range prediction; Model errors; Flood events

1. Introduction

Precipitation is one of the most critical inputs to short-term hydrologic forecasts. Errors in forecasted rainfall intensity, the size and shape of the region forecasted to receive heavy rainfall, the orientation of the heavy rain in relation to the shape and orientation of the basin, and displacement errors in the position of the rain system all have significant impact on the accuracy of hydrologic forecasts. For short-term hydrologic forecasts, quantitative precipitation estimates (QPE) are used to drive hydrologic models as they provide the most up-to-date information about storm systems (Adams and Dymond 2019a). However, QPE limits the possible lead time of flood warnings because forecasts cannot be made until precipitation is falling or has already fallen. Quantitative precipitation forecasts (QPFs) allow forecasters to issue streamflow predictions prior to precipitation initiation, but errors associated with QPF can be large. Even small errors in QPF placement and intensity can lead to critical flood forecast errors at the watershed scale (Rezacova et al. 2007; Knebl Lowrey and Yang 2008; Hapuarachchi et al. 2011; Adams and Dymond 2019a).

Despite significant advances in numerical weather prediction, several challenges remain. Herman and Schumacher (2016) found that extreme precipitation events were generally over predicted for two short-term convection allowing models (CAMs), the High-Resolution Rapid Refresh (HRRR) and the North American Mesoscale 3-km Nest. Further, model QPF is least skillful in the warm season (JJA) due to the convective nature of precipitation at that time and its dependance on weak, small-scale forecasting mechanisms that may not be resolved or even sampled by observational networks (Gallus 2012; Sukovich et al. 2014). Unfortunately, the warm season is when flash flooding is most common in the central United States and the lead time afforded by QPF is most critical.

Several studies have reinforced the notion that QPF skill is insufficient for use in hydrological forecasting. Seo et al. (2018) examined HRRR QPF as input into the Hillslope Link Model (HLM) for prediction of the eastern Iowa floods of 2016. The HLM gave an erroneous discharge peak not detected in observed streamflow, and its performance sharply worsened after the first hour, while some recovery occurred into hours five and six. This is possibly a result of the study including an event with a slow-moving supercell in which peak precipitation values did not vary much but locations of precipitation peaks varied significantly contributing to uncertainty. From an analysis of forecasts for 39 locations within the Ohio River Forecast Center region, Adams and Dymond (2019b) conclude that use of QPF for hydrologic forecasting should be limited to the 6–12-h lead-time forecast because errors increase significantly beyond 12 h. They further observed that fast responding basins are the most sensitive to QPF errors, suggesting that inaccuracies in QPFs have a more detrimental impact in basins that are more prone to flash flooding. Errors in precipitation intensity and timing have been shown to propagate linearly through the hydrologic forecast system (Knebl Lowrey and Yang 2008), which eases the ability to characterize these errors and apply corrections through pre- or postprocessing. However, Knebl Lowrey and Yang (2008) found that location errors will be more difficult

Corresponding author: William A. Gallus, wgallus@gmail.com

DOI: 10.1175/JHM-D-21-0076.1

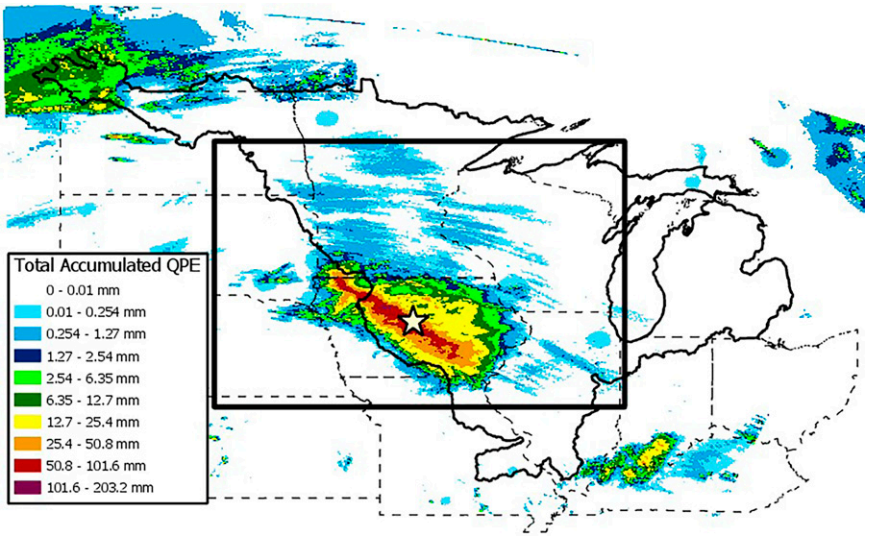

FIG. 1. The NCRFC domain (thin black lines) and the case subset (thick black lines), with example 0–18-h accumulated QPE ending 1800 UTC 18 Jun 2018, and center of mass (white star).

to manage in operational flood prediction because location errors are difficult to predict, and their effects are nonlinear.

Because of the challenges in accurately predicting warm season precipitation with deterministic models, ensemble forecasts are increasingly used to improve QPF skill. Experiments from the Community Leveraged Unified Ensemble (Clark et al. 2018), among others (e.g., Clark et al. 2009), showed that convective allowing ensembles (CAEs) gave a better forecast than convection parameterizing ensembles for warm season precipitation. Despite the advantages that are associated with the use of QPF ensembles, they are not immune to displacement biases (Xuan et al. 2009). For example, Nielsen and Schumacher (2016) found that most members of an ensemble generated by the WRF-ARW were unsuccessful in capturing the location of the south-central Texas flash flood of 25 May 2013, displacing most precipitation to the northwest of observations.

Debiasing and model-error representation (Berner et al. 2015) can improve issues related to spatial errors if a consistent method of doing so can be found. Hardy et al. (2016) present a methodology to account for QPF location uncertainties in the University of Oklahoma's multimodel storm-scale ensemble forecast (SSEF) when applied to probabilistic flash flood forecasting. They first characterize errors in the structure, amplitude, and location of each QPF ensemble member for every hour in the 3-yr analysis period. The QPF error analysis is then combined with the predicted probability of exceedance for each grid in the hydrologic forecast model domain, which is based on the model run using the probability matched mean precipitation forecast and a model reanalysis of return periods for each grid. The resulting flash flooding exceedance probabilities suggest an improved prediction of the area under threat up to 18 h in advance. More recently, Carlberg et al. (2020) examined an approach to mitigate likely displacement errors in high-resolution QPFs by systematically shifting each member by predetermined directions and distances, while retaining the storm morphology of each ensemble member. In that study, the nine members of the HRRR Ensemble (HRRRE) were moved 55.5 km in each of the four cardinal directions and 110 km in each of the four intercardinal directions, expanding the precipitation ensemble size from 9 to 81 members. Each of the 81 members were used as input to the distributed Hydrologic Laboratory-Research Development Hydrologic Model to produce an ensemble streamflow forecast. The ensemble using the shifted QPFs had a higher containing ratio and greater probability of detection for predictions of peak discharge compared to the original unshifted ensemble, and thus better predicted flood occurrence. However, the false alarm ratio did not improve, likely because shifting multiple QPF ensemble members increased the potential to place heavy precipitation in a basin where none occurred. In a preliminary assessment, Carlberg et al. (2020) showed that the ranked probability scores of the streamflow ensembles were improved when the members were weighted according to the most likely direction of displacement of the HRRRE members.

Past studies suggest that more information about displacement errors in QPF is needed to better understand the impact on streamflow forecast skill (Knebl Lowrey and Yang 2008; Hapuarachchi et al. 2011; Adams and Dymond 2019b) and to develop schemes to account for displacement errors in real time (Hardy et al. 2016; Carlberg et al. 2020). The objective of this study is to better characterize the displacement errors in anticipation of using this information to improve short-term hydrologic forecasting. QPFs from two CAEs, the HRRRE and the High-Resolution Ensemble Forecast (HREF), are analyzed. In addition, the present study also explores if displacements present at QPF initiation time are indicative of the overall displacement of the main rainfall region through the first 18 h after model initialization. If a correlation exists,

TABLE 1. Configurations details of HRRRE and HREF. See Dowell et al. (2018) and Benjamin et al. (2016) for more details about HRRRE, and Jirak et al. (2018) for more details about HREF.

Model ensemble	HRRRE	HREF			
Dynamical core	WRF-ARW	HRW-ARW	HRW-NSSL	HRW-NMMB	NAM-NEST
Number of members	9	2	2	2	2
Microphysics	Thompson and Eidhammer (2014)	WRF single-moment 6-class (Hong et al. 2004)	WRF single-moment 6-class (Hong et al. 2004)	Ferrier–Aligo (Aligo et al. 2018)	Ferrier–Aligo (Aligo et al. 2018)
Initial conditions/ boundary conditions	RAP/RAP	RAP/GFS	NAM/NAM	RAP/GFS	NAM/NAM
Planetary boundary layer/surface scheme	Mellor–Yamada–Janjić (Janjić 1990)	Mellor–Yamada–Nakanishi–Niino (Nakanishi and Niino 2009)	Yonsei University (Hong et al. 2006)		
Mellor–Yamada–Janjić (Janjić 1990)		Mellor–Yamada–Janjic (Janjić 1990)			
Member generation	Random perturbations of soil moisture, wind, and water vapor	Normal and time-lagged initial condition	Normal and time-lagged initial condition	Normal and time-lagged initial condition	Normal and time-lagged initial condition
Grid spacing	3 km × 3 km	3 km × 3 km	3 km × 3 km	3 km × 3 km	3 km × 3 km

TABLE 2. List of cases used and ensemble initialization times.

Date	Initialization hour
2 May 2018	0000 UTC
3 May 2018	0000 UTC
4 May 2018	0000 UTC
12 May 2018	0000 UTC
14 May 2018	0000 UTC
23 May 2018	0000 UTC
14 Jun 2018	0000 UTC
16 Jun 2018	0000 UTC
16 Jun 2018	1200 UTC
17 Jun 2018	0000 UTC
17 Jun 2018	1200 UTC
18 Jun 2018	0000 UTC
18 Jun 2018	1200 UTC
20 Jun 2018	0000 UTC
20 Jun 2018	1200 UTC
21 Jun 2018	0000 UTC
24 Jun 2018	1200 UTC
26 Jun 2018	1200 UTC
30 Jun 2018	1200 UTC
1 Jul 2018	0000 UTC
19 Aug 2018	1200 UTC
24 Aug 2018	1200 UTC
26 Aug 2018	1200 UTC
27 Aug 2018	1200 UTC
28 Aug 2018	1200 UTC
2 Sep 2018	1200 UTC
3 Sep 2018	1200 UTC
4 Sep 2018	0000 UTC
4 Sep 2018	1200 UTC
5 Sep 2018	0000 UTC

the displacement for the first hour of QPF accumulation after the event initiates could be a means to preprocess the hydrologic forecasts in real time as precipitation is observed, yet early enough to still improve forecast lead time. We first discuss the study region and how we found case subregions (section 2a), followed by how we analyzed precipitation displacement errors (section 2b), the results of precipitation displacement errors (section 3a), and possible correction strategies of the precipitation displacement errors observed (section 3b). We then conclude and discuss the implications of our results (section 4).

2. Methods

a. Study regions and data

The domain of study was the North Central River Forecast Center (NCRFC) area of responsibility (Fig. 1). The HRRRE and HREF ensembles were chosen because they were the primary CAEs run operationally or in support of research projects in 2018. Also, their fine grid spacing resolves smaller-scale features likely important to hydrological forecasting in small basins. See Table 1 for details on HRRRE and HREF model configurations. Note that after 3 April 2019 HREF was expanded to include an additional model (the operational HRRR) at the same two times, extending it to 10 members (Storm Prediction Center 2019). This new ensemble was not

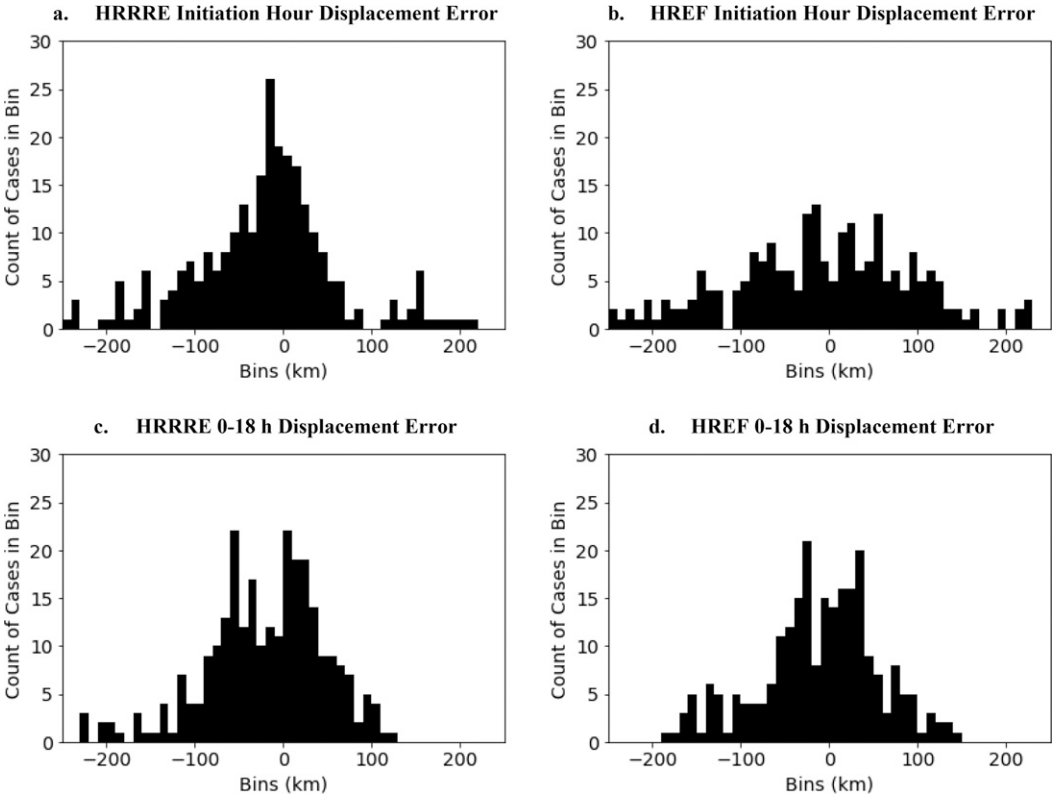

FIG. 2. Histograms of east–west (a) HRRRE initiation hour displacement errors, (b) HREF initiation hour displacement errors, (c) HRRRE 0–18-h displacement errors, and (d) HREF 0–18-h displacement errors. Histogram bin edges are every 10 km starting at −250 km and ending at 250 km.

represented in the present study. HREF data were obtained through an archive at the National Severe Storms Laboratory (Roberts 2018, personal communication) and are on a ~3-km grid.

The QPE used for verification was the Multisensor Precipitation Estimator (Seo and Breidenbach 2002), an operational product that was obtained from the NCRFC. The QPE was stored on a 4 km ×4 km grid. The HRRRE and HREF were likewise bilinearly interpolated to the same 4 km × 4 km grid.

The present study analyzed 30 separate cases (Table 2). For a case to be included, a rainfall event had to be sufficient to cause issuance of either a flash flood watch or warning within the NCRFC area. Further, forecasted accumulated precipitation data had to be available for both HRRRE and HREF at the same initialization time, and the precipitation of interest had to fall primarily in the first 18 h of the model runs. The 30 cases were all from the warm season of 2018, with the earliest occurring on 2 May 2018 and the latest occurring on 5 September 2018. Although a larger sample size would be helpful, these were the only events meeting the above criteria for the region over which our research project was focused during the warm season of 2018. That year was especially wet in this part of the country and provided substantially more cases than would be available in a more typical warm season and provided a good sample size of events. For each case, we manually selected a polygon, or subset of the QPF, on which to focus the analysis. The polygon boundaries followed lines of constant latitude/longitude or the edge of the QPE dataset, were made to be rectangles as frequently as possible, and included only the system whose QPE/QPF contributed to the flash flood watch/warning. Figure 1 shows the subset for the 1800 UTC 18 June 2018 case.

As might be expected for events that led to issuance of flash flood watches or warnings, 29 of the 30 cases involved convection that grew upscale to meet the definition of a mesoscale convective system (a continuous band of at least 100 km in length of radar reflectivity exceeding 40 dBZ). Strong large-scale forcing (defined as a 500-mb trough or cutoff low overhead or within 1000 km upstream of the rain event or a strong frontal signature at 850 mb; 1 mb = 1 hPa) with flow exceeding 30 kt (1 kt ≈ 0.51 m s^{-1}) at 500 mb, or 20 kt at 850 mb, was present in 80% of the cases. Based on Jankov and Gallus (2004) and Squitieri and Gallus (2016), among others, it is likely that our sample of cases represents relatively well-predicted events, since forecast skill is greater when large-scale forcing is stronger. Displacement errors would likely be greater for events with weaker forcing, and because these events are not as predictable, they are not the focus of the present study.

b. *Precipitation displacement analysis*

For each case, we calculated the center of mass, or centroid, of the precipitation region (defined as grid points with at least

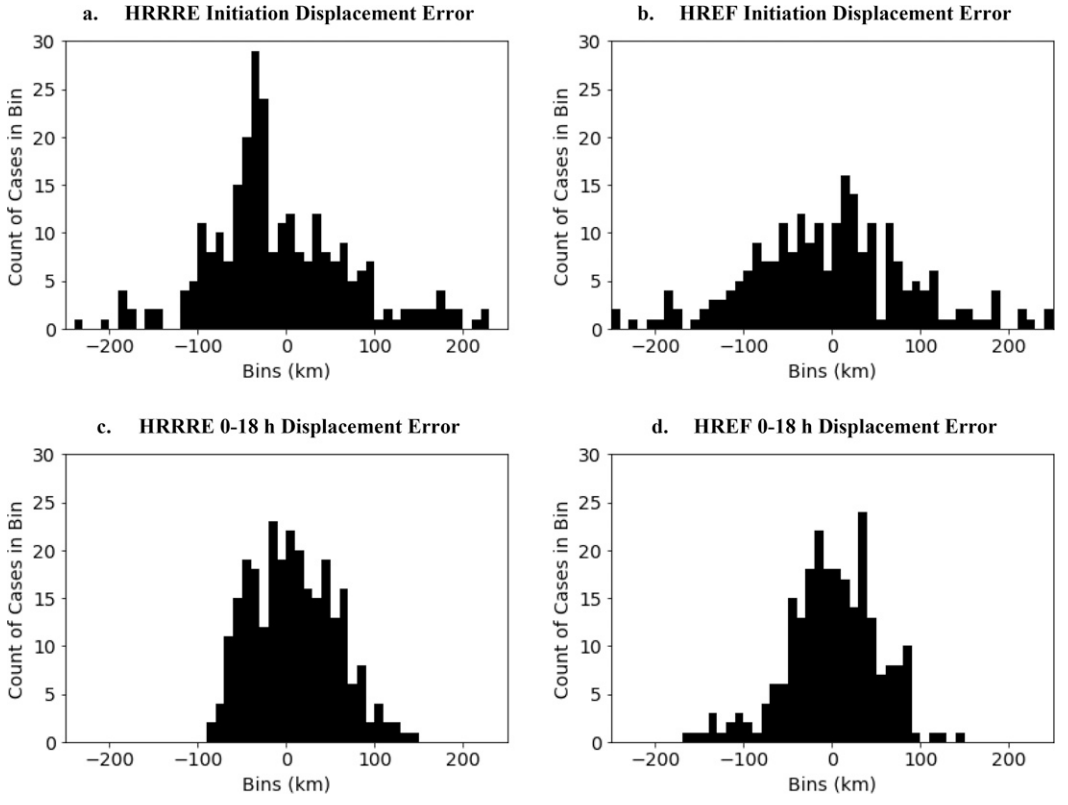

FIG. 3. As in Fig. 2, but for north–south displacement errors.

1 mm of precipitation), for the first 18 h after model initialization (hereafter, 0–18-h accumulation period). The centroid of the "initiation hour" accumulation was also computed, where "initiation hour" was defined as the first hour in the forecast period when the areal extent of hourly QPE/QPF greater than 1 mm exceeded 1000 km^2, a maximum rate of at least 10 mm h^{-1} was present within the area, and either the area of 1-mm rainfall increased, or the intensity of the peak rainfall in the system increased for at least three consecutive hours. The criteria for initiation hour were determined subjectively by analyzing the hourly progression of each case and selecting the time when the initiation hour criteria were satisfied. Although the HREF and HRRRE members provided forecasts for 36 h for all cases, we focused on only the first 18 h of the simulations, because we chose model initialization times so that the primary rain event occurred in the first 18 h. This choice allowed us to focus on the part of the model runs that typically have more skill, as model errors typically grow with time. In 19 of the 30 events, the rainfall system initiation hour was also the first hour after the model initialization. In all cases, the initiation happened by the eighth hour of the forecast. The fact that initiation happened so frequently at the first hour is mainly a result of our case selection and methodology and is not an indication of a problem in the ensembles whereby anomalous precipitation occurs at initialization. Observations of rainfall timing matched well with what was occurring in the ensembles. An example of a center of mass with 0–18-h accumulated QPE is provided (Fig. 1).

TABLE 3. Ratio of the QPF displacement for the 0–18-h period compared to the initiation period listed by the quadrant in which the displacement occurred at precipitation initiation. Ratios are given for both the north–south (N–S) and east–west directions (E–W).

Quadrant of displacement at precipitation initiation	HRRRE		HREF	
	N–S	E–W	N–S	E–W
NW	0.70	0.58	0.32	0.19
NE	0.35	0.54	0.17	0.07
SW	0.15	0.49	0.02	0.28
SE	0.33	0.17	0.52	0.02

After a center of mass was determined for both the observed system and each ensemble member, the north–south and east–west components of the displacement error for both the initiation hour and the 0–18-h accumulation period were computed. Specifically, we compute the displacement error as the latitude or longitude of the QPE centroid minus the latitude or longitude of the model QPF centroid. Thus, a positive value indicated a northward/eastward displacement relative to the observed centroid, and a negative value indicated a southward/westward displacement from the observed centroid. The displacement errors (Figs. 2 and 3) suggested a

TABLE 4. Mean and standard deviation of displacement of the QPF centroids from the HRRRE and HREF ensemble members as compared to the centroid of the QPE for the initiation hour and the 0–18-h accumulation periods.

	Initiation hour displacement		0–18-h accumulation displacement	
Model	Mean (km)	Standard deviation (km)	Mean (km)	Standard deviation (km)
HRRRE	105.2	79.5	72.2	43.1
HREF	148.8	102.6	72.1	45.7

normal distribution. We chose to use a two-tailed Student's *t* test to determine if statistically significant displacement errors were present in the data. Means and standard deviations of displacement errors were compared from the HRRRE and HREF to understand their relative accuracy in predicting the location of precipitation systems. In addition, the Pearson's correlation coefficient was computed between the 0- and 18-h accumulation period displacement errors and initiation hour displacement errors to determine their relationship.

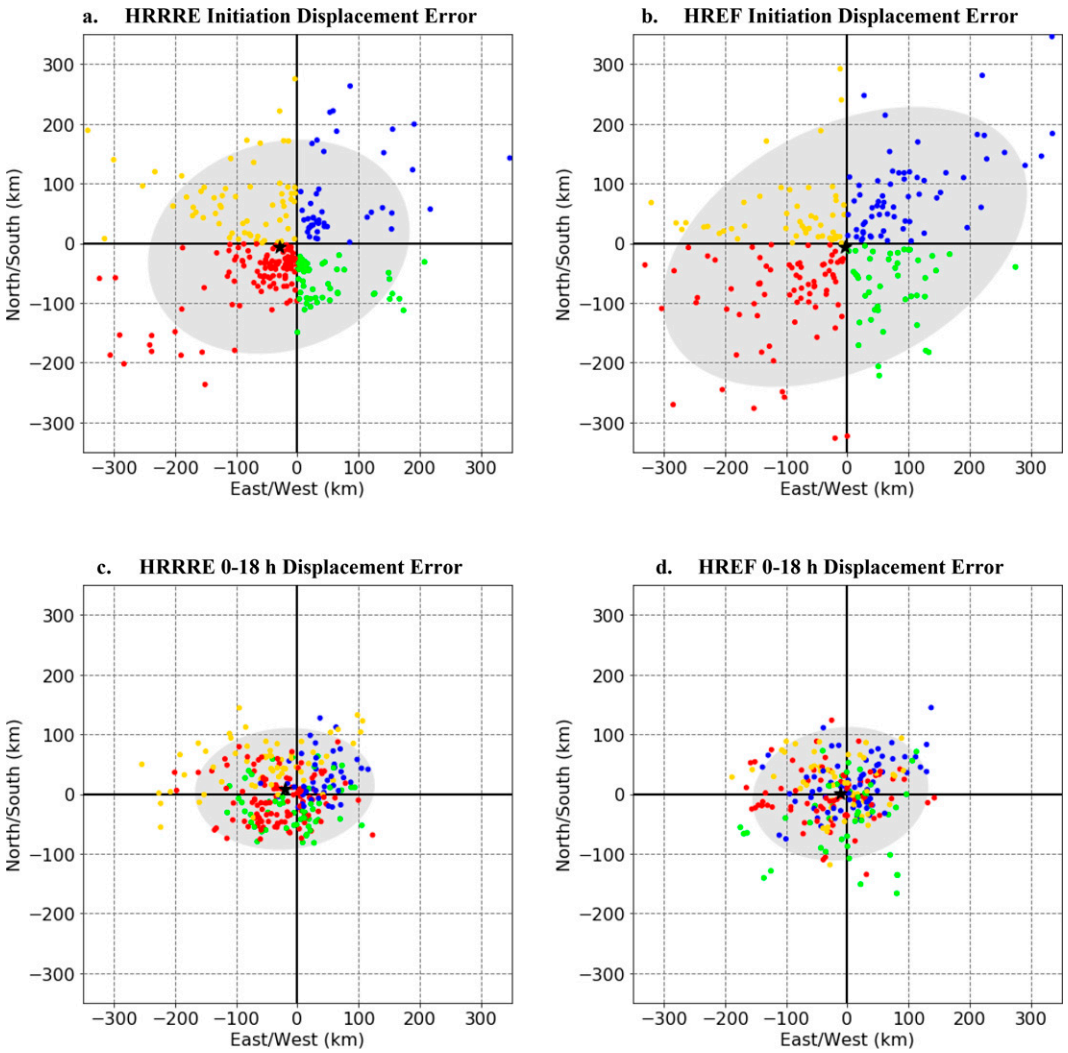

FIG. 4. (a),(c) HRRRE and (b),(d) HREF (top) initiation hour and (bottom) 0–18-h accumulation period QPF centroid displacement errors for all members of all cases, graphed by cardinal direction. Points are color coded by the quadrant in which the initiation hour displacements occurred (NW: yellow, NE: blue, SW: red, SE: green). The mean of displacement errors of all cases is marked (black star). The gray shaded area represents a bivariate ellipse that captures 90% of the sample.

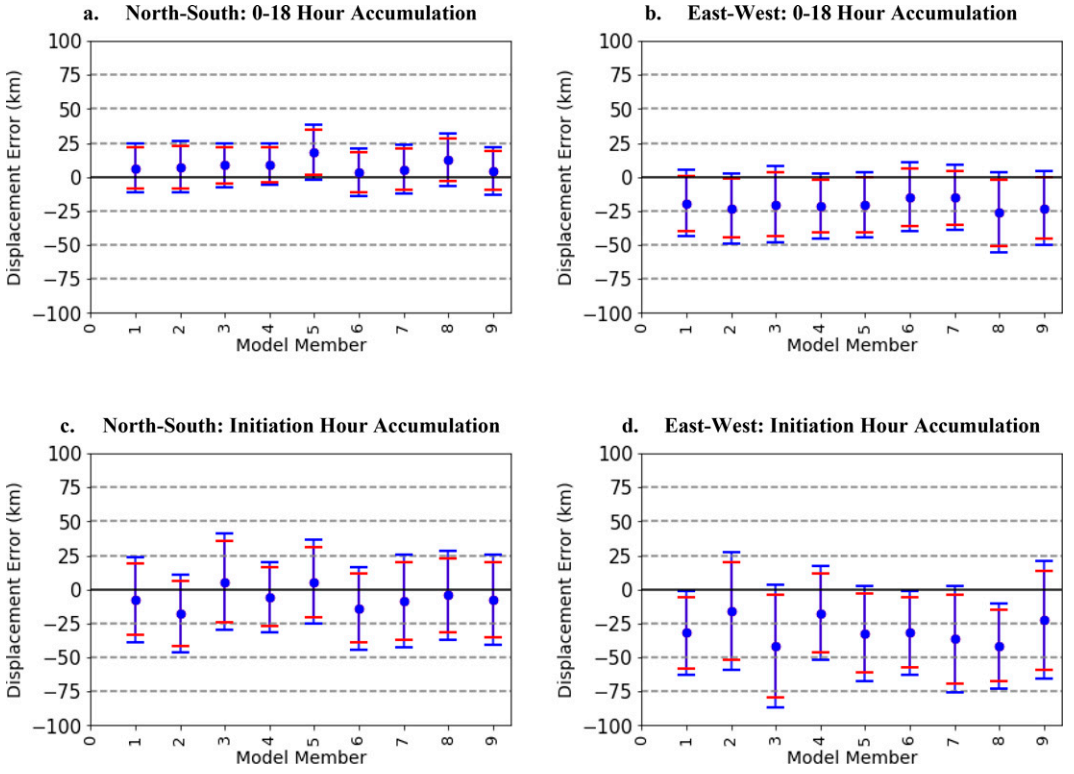

FIG. 5. (a),(c) North–south and (b),(d) east–west mean displacement errors with 95% confidence intervals (blue bars) and 90% confidence intervals (red bars) for every ensemble member of HRRRE showing (top) 0–18-h accumulation displacement errors and (bottom) initiation hour displacement errors. Positive (negative) values indicate northward (southward) or eastward (westward) displacements.

After displacement errors were determined, three methods were explored to see if the displacement errors in the 0–18-h precipitation system could be reduced:

1) Adjust the location for an event-total precipitation field based on the displacement error present when the system first formed. The north–south components of the 0–18-h QPF centroid were subtracted by the north–south components of the initiation hour QPF displacement errors, and likewise for the east–west components. This produced a correction for the position of the centroid of the 0–18-h accumulation period QPF.
2) The approach used in method 1 was altered such that the 0–18-h QPF field was shifted only a fraction of the displacement present in the initiation hour QPF field. To do so, the north–south and east–west 0–18-h QPF displacement components were corrected using a single weight equal to the average distance of displacement for the 0–18-h accumulation period divided by the average distance of displacement for the initiation hour. The weights were 0.769 and 0.511 for HRRRE and HREF, respectively.
3) The approach used in method 2 was followed but with separate weights (Table 3) calculated for each intercardinal direction (NW, NE, SW, SE) where the displacement occurred at initiation hour. For each of these four quadrants, the north–south and east–west components of displacement were computed, and the fraction to shift the original 0–18-h QPF centroid was then calculated in a manner similar to method 2, but by computing the two components independently.

The full sample averages are used in all three tests. Because of the small sample size in the present study, the same 30 cases were used both to determine bias and to verify the impact of adjusting the QPF fields for this bias.

3. Results

a. *QPF displacement analysis*

The mean and standard deviation of the accumulation period QPF displacement errors were similar for both HRRRE and HREF (Table 4). For both ensembles, the initiation hour mean displacement errors and standard deviations were greater than those of the 0–18-h period displacement errors. An analysis of hourly displacement errors (not shown) suggested that in the first few hours after initiation in the HREF ensemble, errors become smaller, possibly because the convective system was growing upscale and larger systems are typically more predictable, especially if they are strongly influenced by larger-scale forcing. However, in both ensembles,

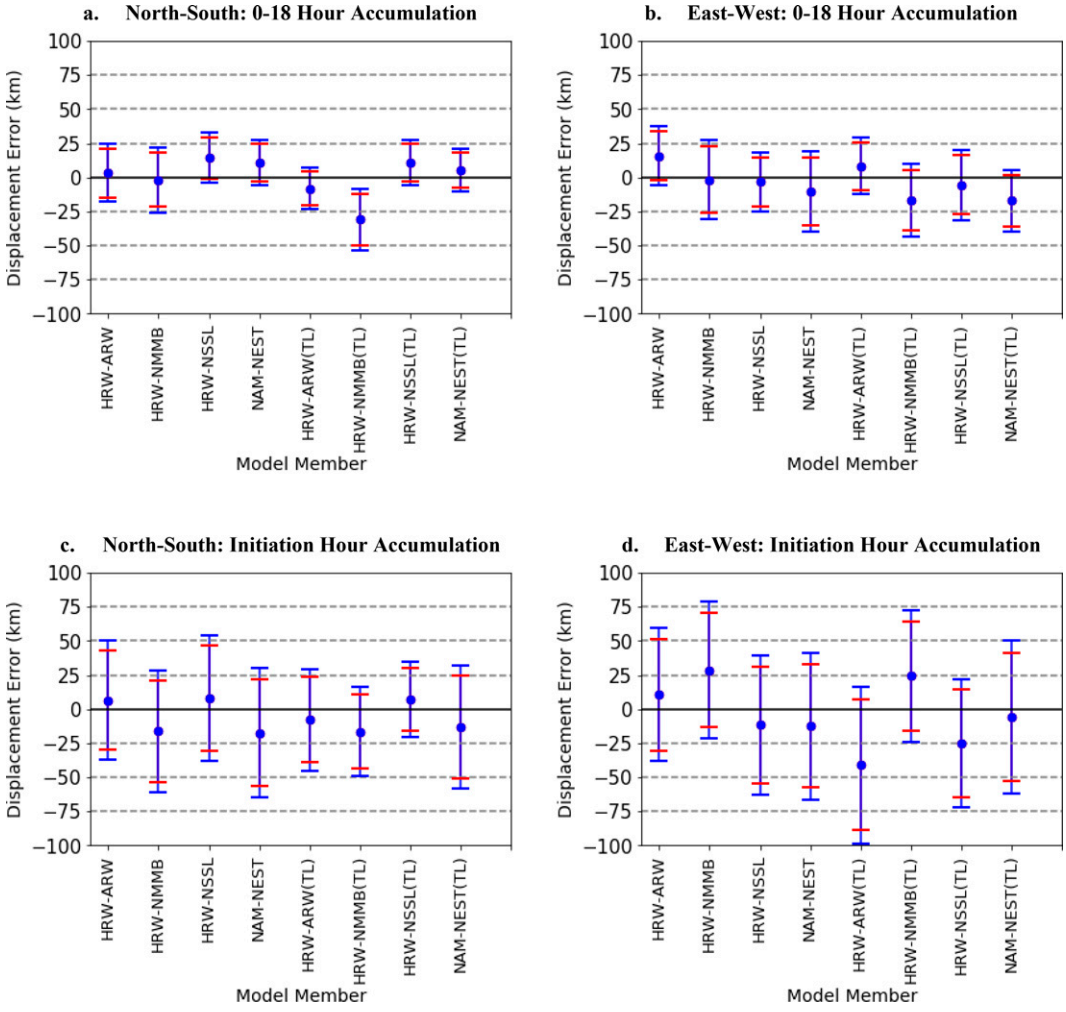

FIG. 6. As in Fig. 5, but for HREF members, including the time-lagged (TL) ensemble members.

hourly displacements were always larger than the full period value, and thus the difference in these values is mostly because forecast errors are reduced when a larger time interval is used. The mean and standard deviation of HREF was greater than those for HRRRE for initiation hour displacement (Table 4). This result is consistent with prior studies that have found that the use of mixed physics or mixed models, as in HREF, results in more spread in short-term forecasts than the use of perturbed initial and lateral boundary conditions alone. (e.g., Stensrud et al. 2000; Hacker et al. 2011; Berner et al. 2011, 2015; Gallus et al. 2019).

Displacement errors for each member of every case were graphed along with a 90% confidence bivariate ellipse (Fig. 4). The trends discussed earlier regarding mean displacement error distances being greater at initiation hour than for the 0–18-h period can be seen with broader ellipses for both HRRRE and HREF. An analysis of the errors of each member for each case shows that the initiation hour values are larger than the 0–18-h period values 72.5% of the time for HREF, and 66.7% of the time for HRRRE. The change in the orientation of the ellipses indicated that a greater reduction occurs in north–south variability among members and cases than with east–west variability when the initiation hour values are compared to those for the 0–18-h period. Furthermore, both HRRRE's 0–18-h and initiation hour displacement errors suggest a general westward bias in the ensemble, as the center of the ellipse is positioned west of the origin (Figs. 5b,d). Such a systematic direction bias does not appear with the HREF data (Figs. 6b,d), although there may be a slight westward bias in the 0–18-h QPF displacements.

We now focus our discussion on HRRRE. Although the mean for all members of HRRRE for the 0–18-h period centroid displacement errors is to the north of the observed centroids for all members (Fig. 5a), the northward position is not significant at the 95% confidence level. Likewise, the north–south initiation hour period displacement is also not significant in either direction (Fig. 5c). The east–west 0–18-h accumulation and initiation hour accumulation displacement errors are not significant at the 95% level (Figs. 5b,d).

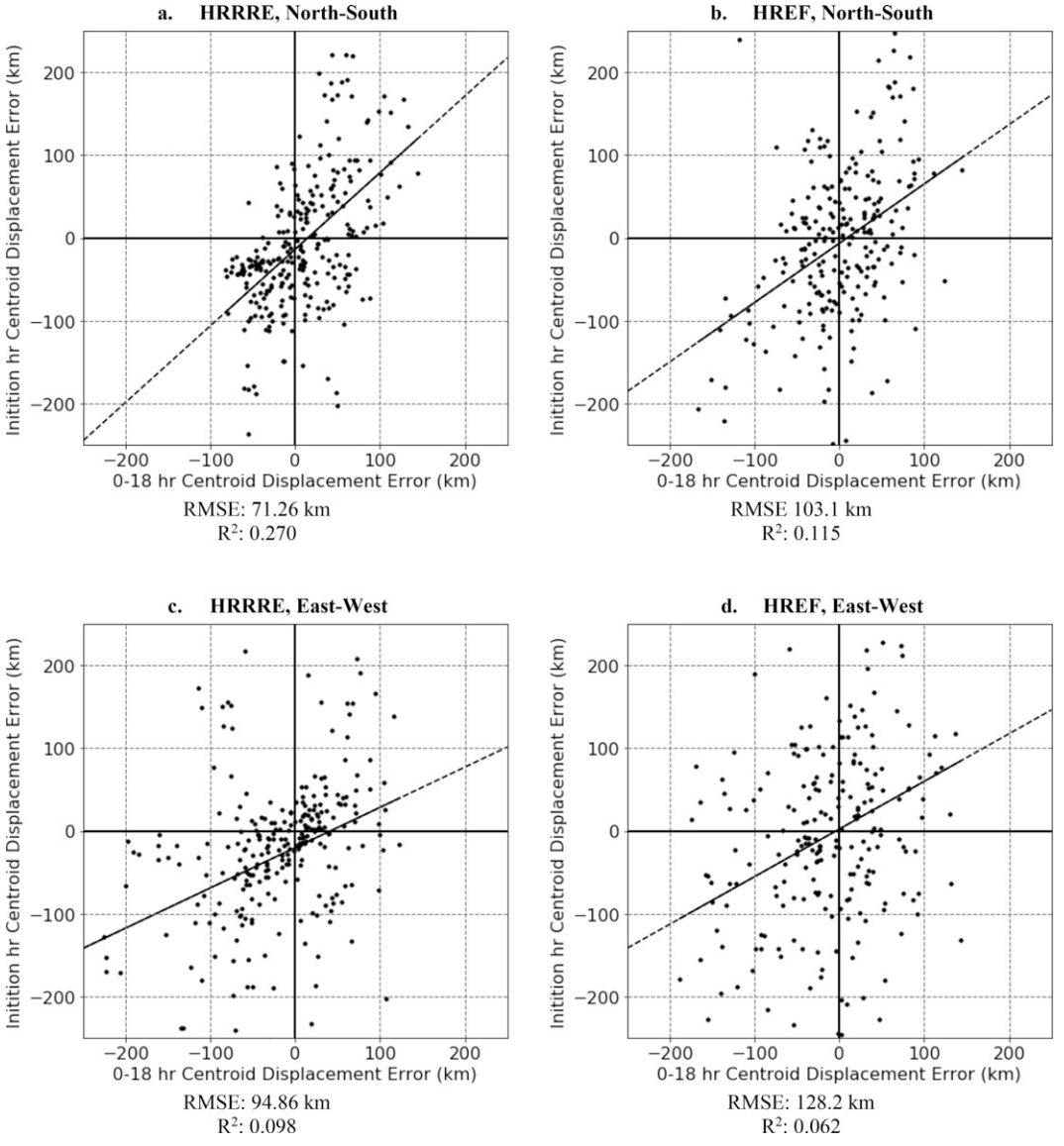

FIG. 7. (a),(c) HRRRE and (b),(d) HREF initiation hour displacement errors vs 0–18-h QPF displacement errors in the (top) north–south and (bottom) east–west directions. Line of best fit (black, solid interpolation, dashed extrapolation), with root-mean-square error (RMSE), and correlation coefficients (R^2) provided below the respective plot.

However, for most ensemble members and both initiation hour and 0–18-h accumulation displacement errors, the westward displacement errors observed are very close to meeting a 95% significance threshold. Furthermore, 5 of 9 and 6 of 9 ensemble members show westward displacement errors at 90% significance for initiation hour accumulations and 0–18-h accumulations, respectively. Of note, the members with the most significant errors during the initiation hour were not always the members with the most significant systematic errors for the 0–18-h period (Fig. 5).

For HREF, 0–18-h QPF centroids were usually displaced a little north of the observed system in most members (Fig. 6a) but results were generally not significant, except for a southward bias for the time-lagged Nonhydrostatic Mesoscale Model on B-grid (NMMB). Additionally, more members showed a westward bias than an eastward bias, but none of the east–west biases were statistically significant at the 95% confidence level (Fig. 6b). For initiation hour, HREF members were more often displaced to the south (Fig. 6c) and the west (Fig. 6d) but not significantly. The east–west displacement errors were more variable for the HREF members than the HRRRE members. In both ensembles, the reduction in the magnitude of the displacement errors (Table 3) present in the 0–18-h accumulation periods compared to the initiation hour accumulations varied by quadrant and was usually more than 50%.

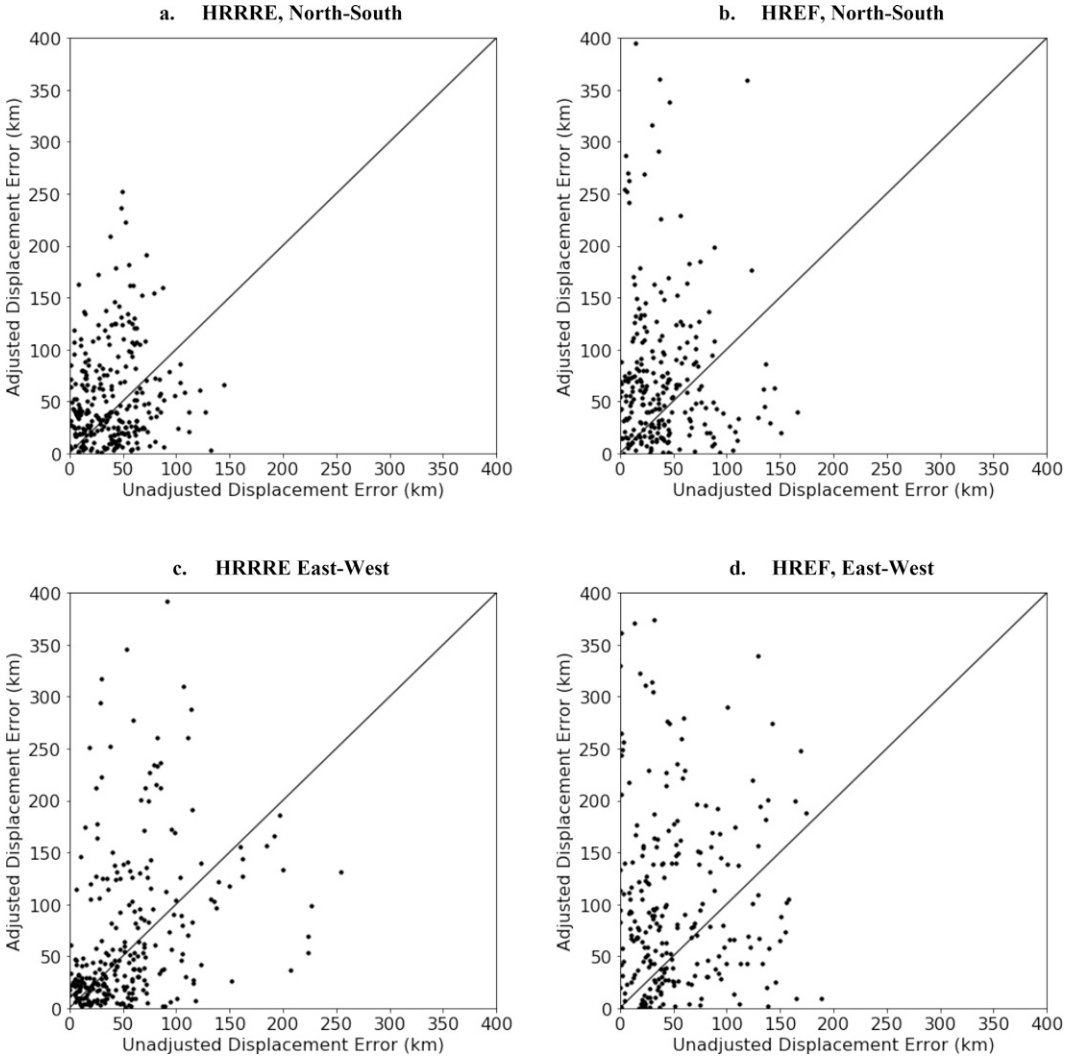

FIG. 8. (a),(c) HRRRE and (b),(d) HREF 0–18-h QPF displacement errors vs 0–18-h QPF displacement errors present after adjusting the centroid using the initiation hour displacement errors for the (top) north–south and (bottom) east–west directions (method 1). The 1:1 line is drawn for reference. Points above the line indicate the adjustment made the displacement error worse, and points below the line indicate an improvement in the displacement error.

b. *Potential for applying displacement analysis in forecasting*

The analysis described above suggests it may be possible to improve some forecasting techniques that use the HRRRE ensemble based on typical displacement errors because a systematic bias is present in the westward direction. However, a substantial amount of spread existed in all four directions among cases and there was no preferred displacement in the north–south direction. Because there was no apparent directional bias in the HREF members, anticipating displacement errors in advance may not be possible when using these forecasts. The overall lack of a clear systematic bias in both direction and distance of displacement for the centroids of precipitation systems in the ensemble members suggests that techniques other than directly applying the displacement error when a system first forms as in method 1 of section 2b may be needed to account for spatial errors in QPFs. The results from testing several different techniques are described below.

1) DISPLACEMENT CORRECTION 1

For applications such as hydrologic forecasting the approach described in method 1 of section 2b would not offer as much lead time as one that could anticipate displacement errors prior to the start of rain based on known accumulation biases. However, the method would allow more lead time than current operational practices that use QPE after a large portion of the precipitation has already fallen. Figure 2 suggested that there may be some relationship between the displacement errors of the QPF during the initiation hour of a system and the QPF for the full 0–18-h period. To check the relationship, we plotted the 0–18-h QPF centroid

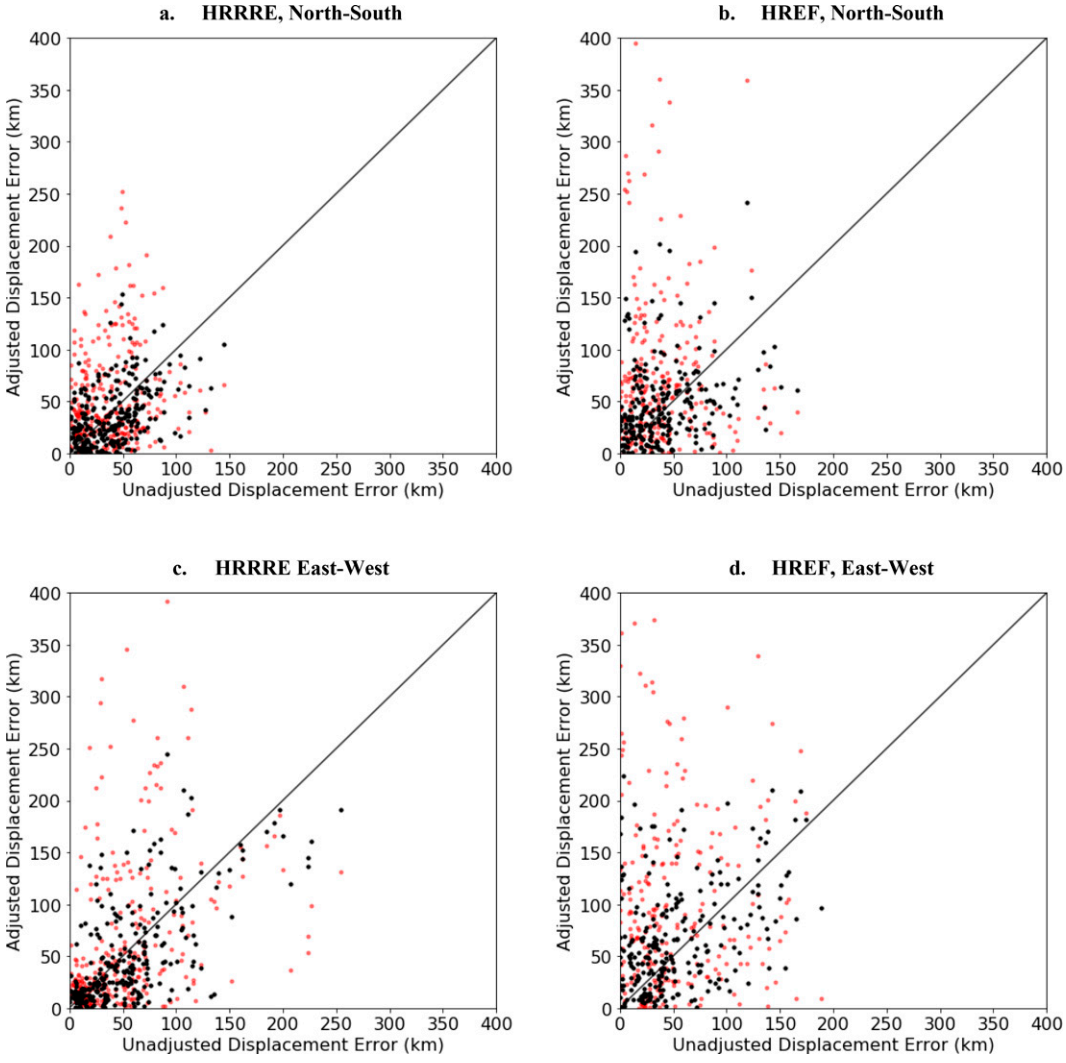

FIG. 9. As in Fig. 8, but with the correction to the 0–18-h QPF centroid based on shifting the centroid by a fraction of the initiation hour displacement amount where the fraction is equal to the mean of the 0–18-h QPF displacement errors divided by the mean of the initiation hour displacement errors (method 2). Plotted in red is Fig. 8, for reference.

displacement errors versus the initiation hour displacement errors (Fig. 7). A very weak positive correlation was noted for both HRRRE and HREF, with HREF's correlation being especially weak.

The weak correlation (Fig. 7) encouraged us to explore whether using the initiation hour displacement error would help to correct the 0–18-h accumulation displacement error. Our first adjustment attempt used method 1 as described in section 2b (Fig. 8). However, using method 1 resulted in more ensemble members having a higher displacement error after adjustment; 152 of the 270 (56%) events and 137 of the 270 (51%) events simulated by HRRRE had higher north–south and east–west displacement errors, respectively. For HREF, 159 of 240 (66%) events, and 156 of 240 (65%) events had higher north–south and east–west displacement errors, respectively. These results show that this adjustment did not help to improve displacement errors for the 0–18-h period. Figure 4 suggests that these worse displacement errors may be because the initiation hour displacements were usually much larger than the 0–18-h QPF displacement errors, so that even if the full system QPF field ends up displaced in the same direction as that of the initiation hour QPF field, the resulting adjustment overcorrects the QPF field.

2) DISPLACEMENT CORRECTION 2

The weight calculated by the method described in method 2 of section 2b accounted for the fact that initiation hour displacements were larger on average than the full period displacements. This adjustment also assumed isotropic behavior in the differences between initiation hour displacement magnitude and the full period displacement magnitude (Fig. 9). In

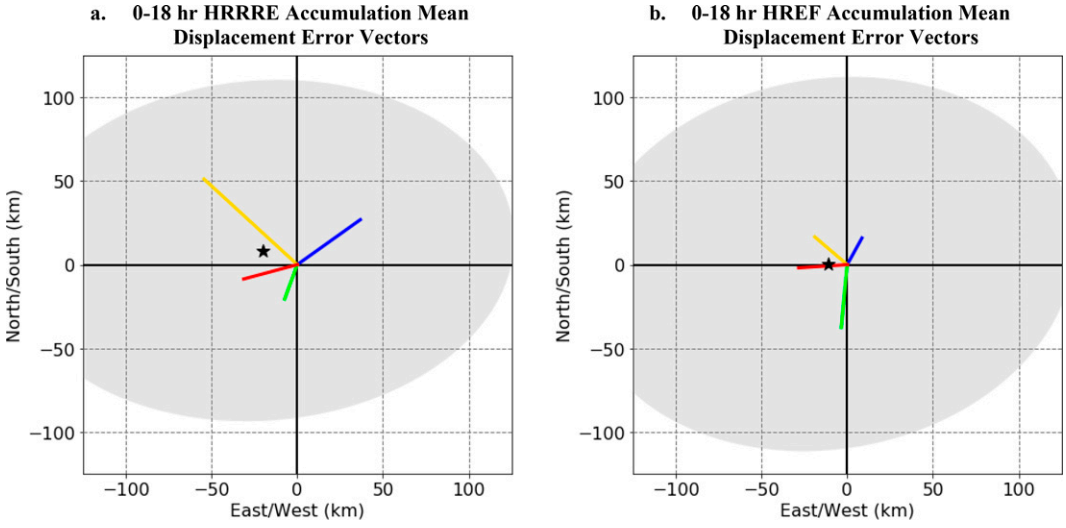

FIG. 10. 0–18-h vectors pointing from the origin to the mean of each quadrant in (a) Fig. 4c and (b) Fig. 4d, with shading indicating the corresponding bivariate ellipses, that is, NW: yellow, NE: blue, SW: red, SE: green.

this case, 124 of 270 (46%) events, and 121 of 270 (45%) events simulated by HRRRE had higher north–south and east–west displacement errors, respectively. For HREF, 131 of 240 (55%) and 137 of 240 (57%) events had higher north–south and east–west displacement errors for HREF, respectively. Although fewer data points were found above the diagonal line, implying some tendency for more cases to improve using this approach, around as many model members showed an improvement as did not, indicating uncertainty that the strategy would work to improve the 0–18-h period displacement errors over what they were originally.

3) DISPLACEMENT CORRECTION 3

As can be seen in Fig. 4, there was some tendency for systems to remain displaced in the same quadrant where they were initially displaced with 66%, 67%, 40%, and 35% of HRRRE members and 42%, 39%, 39%, and 40% of HREF members remained in the northwest (NW), northeast (NE), southwest (SW), and southeast (SE) quadrants, respectively. The vectors depicting the mean 0–18-h accumulation centroid displacement error quadrants for member sets that have the same directional displacement error at initiation are plotted, except for the SE vector which plotted into the SW quadrant (Fig. 10). HRRRE showed a stronger tendency to remain in the original quadrant than HREF, but with the percentage of members that remained in the original quadrant exceeding 25% (random selection of a quadrant) for both ensembles, the method described in method 3 of section 2b is worth exploring.

Results are presented for each the NW (Fig. 11), NE (Fig. 12), SW (Fig. 13), and SE (Fig. 14) quadrants. Detailed statistics of how method 3 of section 2b improved displacement errors are described in Table 5 (north–south) and Table 6 (east–west). Most quadrant corrections resulted in

TABLE 5. Table depicting number of times method 3 of section 2b improved displacement errors for each quadrant, for north–south component of displacement errors. This is a numerical summary of results shown in Fig. 11 (NW), Fig. 12 (NE), Fig. 13 (SW), and Fig. 14 (SE).

Quadrant	Number of improved displacement errors	Total number of members	Percent
HRRRE			
NW	42	61	69%
NE	31	45	69%
SW	64	110	58%
SE	35	54	65%
HREF			
NW	32	50	64%
NE	40	69	58%
SW	43	76	57%
SE	27	45	60%

TABLE 6. As in Table 5, but for east–west component of displacement errors.

Quadrant	Number of improved displacement errors	Total number of members	Percent
HRRRE			
NW	41	61	67%
NE	34	45	76%
SW	67	110	61%
SE	25	54	46%
HREF			
NW	28	50	56%
NE	40	69	58%
SW	43	76	57%
SE	18	45	40%

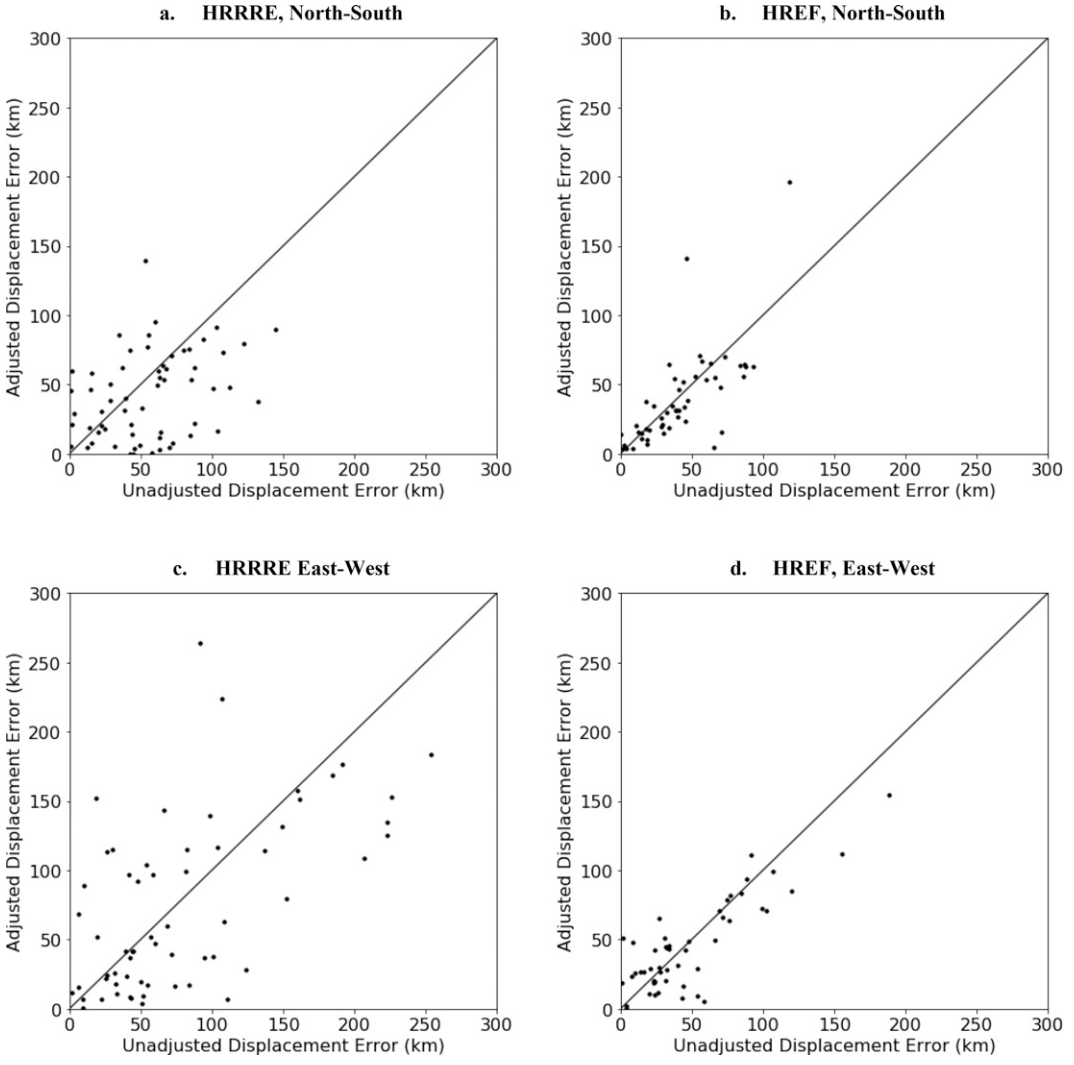

FIG. 11. As in Fig. 8, but for method 3, but only for cases where the initiation hour displacement was in the NW quadrant, with the 0–18-h QPF centroid position shifted separately in the north–south and east–west directions by a fraction of the initiation hour displacement amount, where the fraction is equal to the 0–18-h QPF centroid displacement errors in both directions divided by the initiation hour displacement errors in both directions.

either a majority of cases having improved displacement errors, or very small fractional shifts (as noted in Table 3). Displacement errors were improved more frequently than made worse. Table 7 gives the resulting Student's t test p values for each quadrant. The p values for the HRRRE adjustments showed that the displacement errors of the adjusted 0–18-h QPF field were significantly smaller than those in the original 0–18-h QPF field, with 95% confidence met for the north–south component in all quadrants except southwest, but such confidence was only met for the east–west component in the southwest quadrant. For HREF, this technique also improved the displacement errors for the north–south component with 90% confidence for all quadrants except the northwest, including 95% confidence for the southwest and southeast quadrants, and 95% for the east–west component in the northeast quadrant. We note that due to small sample size, we cannot separate our dataset into training and evaluation datasets.

4. Discussion and conclusions

Based on 30 warm season heavy rainfall events in the NCRFC domain, the QPF displacement errors associated with the centroids of these systems in two commonly used CAEs, the HRRRE and the HREF, were documented, both at 0–18-h period where most of the rain occurred and for the initiation hour when substantial precipitation was first present. The HRRRE members had smaller spread in the placement of precipitation system centroids compared to the HREF at the initiation of precipitation (Fig. 4). This result was not surprising since the HRRRE uses only perturbed initial and lateral boundary conditions to supply diversity among

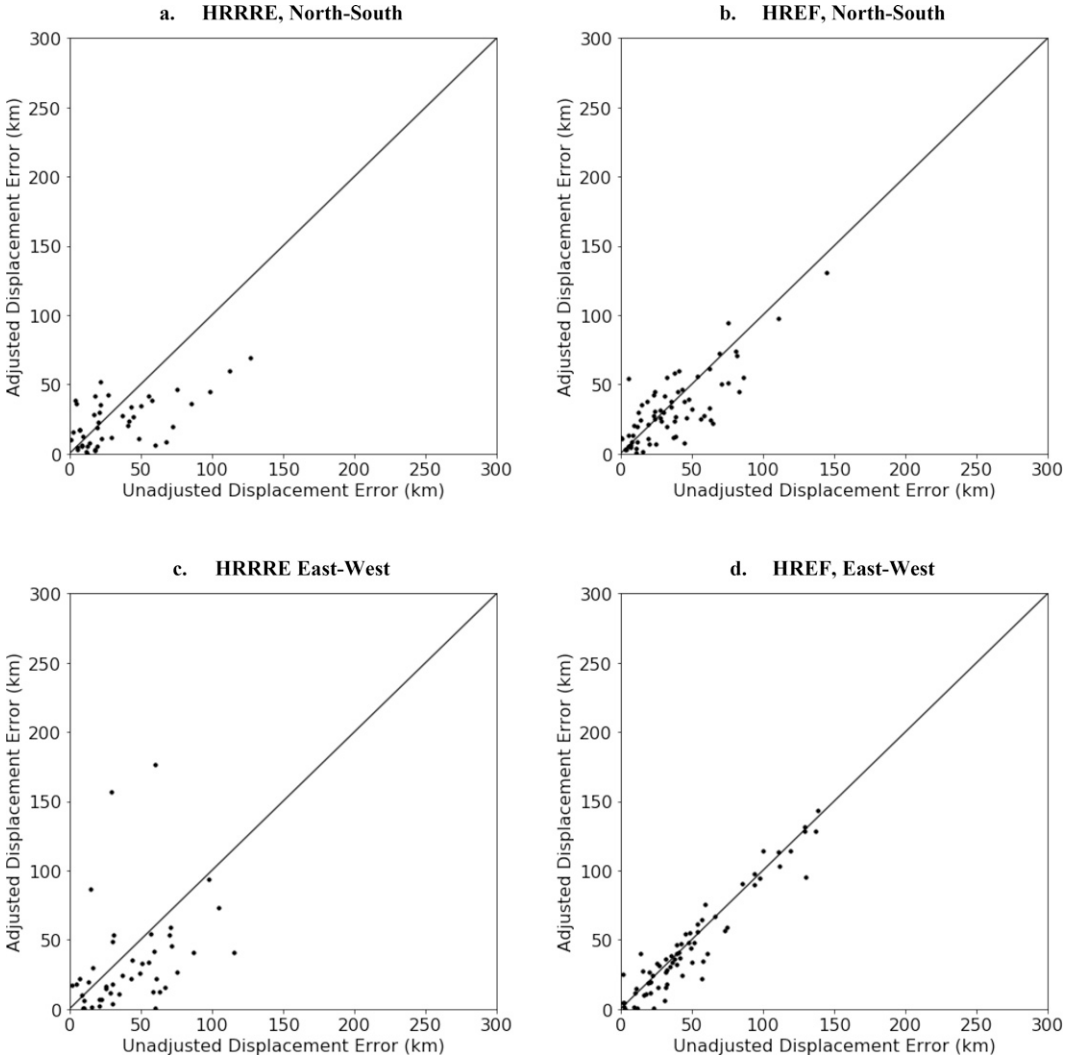

FIG. 12. As in Fig. 11, but for cases where the initiation hour displacement was in the NE quadrant.

its members. In contrast, HREF members uses different model dynamical cores with different physics schemes, and time-lagged members that supply diversity in initial and lateral boundary conditions as well. Perhaps because of the increased spread in HREF, there were no systematic biases in displacement direction observed. Higher randomness of displacement errors in HREF limits the ability to improve forecasts based simply on a climatology of past location errors. For HRRRE, there was a statistically significant displacement toward the west in many members (Fig. 5). However, scatter was large, so it is unlikely a single constant adjustment can be made to the locations of QPF to improve the skill of the HRRRE member QPFs.

Displacement errors for the centroids of precipitating systems present during the initiation hour were usually larger than the displacement errors for the centroids of the 0–18-h accumulated precipitation from the systems, especially in the east–west direction (Fig. 4). Thus, a simple adjustment to the full period precipitation location based on the displacement error at the initiation hour did not improve the forecast position of the full 0–18 h rainfall (Figs. 8 and 9). However, when using a technique based on the quadrant in which the initiation hour displacement error was present (Figs. 11–14), a statistically significant improvement to the north–south and east–west displacement error components of the 0–18-h QPF field occurred in most directions when fractions of the initiation hour QPF displacement error components were subtracted from them (Tables 5 and 6). Thus, forecast positions of 0–18-h precipitation systems in both ensembles are often improved when using the quadrant method to adjust the 0–18-h QPF centroids (Table 7).

A primary motivation for this study was to better understand displacement errors in QPF because errors in the location of precipitation have significant impacts on hydrologic forecast accuracy. The results suggest that it is possible to improve QPF forecasts for the location of heavy rainfall based

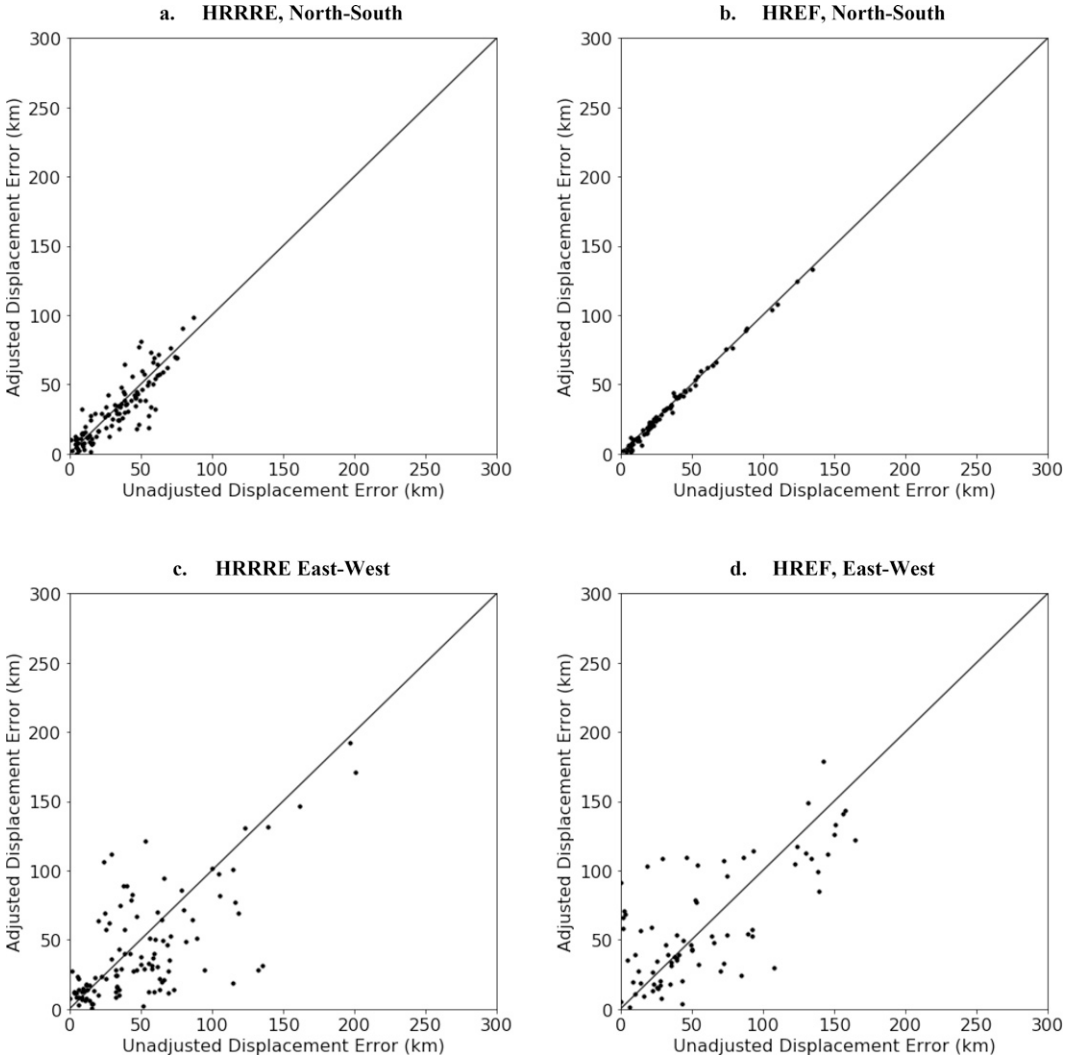

FIG. 13. As in Fig. 11, but for cases where the initiation hour displacement was in the SW quadrant.

upon the displacement error present in the initiating hour of rainfall, even though the displacements of the centroids of the longer-duration precipitation event usually differ somewhat from those of the initiation hour rainfall. Based on this result, streamflow ensemble approaches like that of Carlberg et al. (2020), which shifted QPF to account for uncertainty in displacement, may be improved using weights to update streamflow ensembles based on errors in the initiation hour QPF field. Otherwise, unlike in the southern Plains where forecasters have often noted that models are too quick to move drylines east (e.g., Clark et al. 2015; Coffer et al. 2013), we did not find evidence of clear systematic biases in the direction of QPF displacement errors, and to our knowledge no studies have documented systematic errors in model positioning of weather features in the Upper Midwest. In forthcoming work, we use the results found here to improve the efficiency of the Carlberg et al. (2020) technique by reducing the number of shifts to those that reasonably replicate the observed distribution of displacements and test the impact of ensemble corrections at initiation hour with the National Water Model.

Future work should examine other atmospheric variables to determine if it is possible to anticipate (ideally earlier than the initiation hour) the most likely displacement error based on parameters such as shear, convective available potential energy, and moisture content of the atmosphere. In addition, future studies should include more cases sufficient to separate into training and evaluation datasets and examine regional variability of displacement errors across the United States. Machine learning techniques may prove advantageous to discovering more complex relationships between weather parameters and displacement errors. Finally, verification software such as the Method for Object-Based Diagnostic Evaluation (Davis et al. 2006) could be used to perform analysis of the other components of QPF error including the distribution

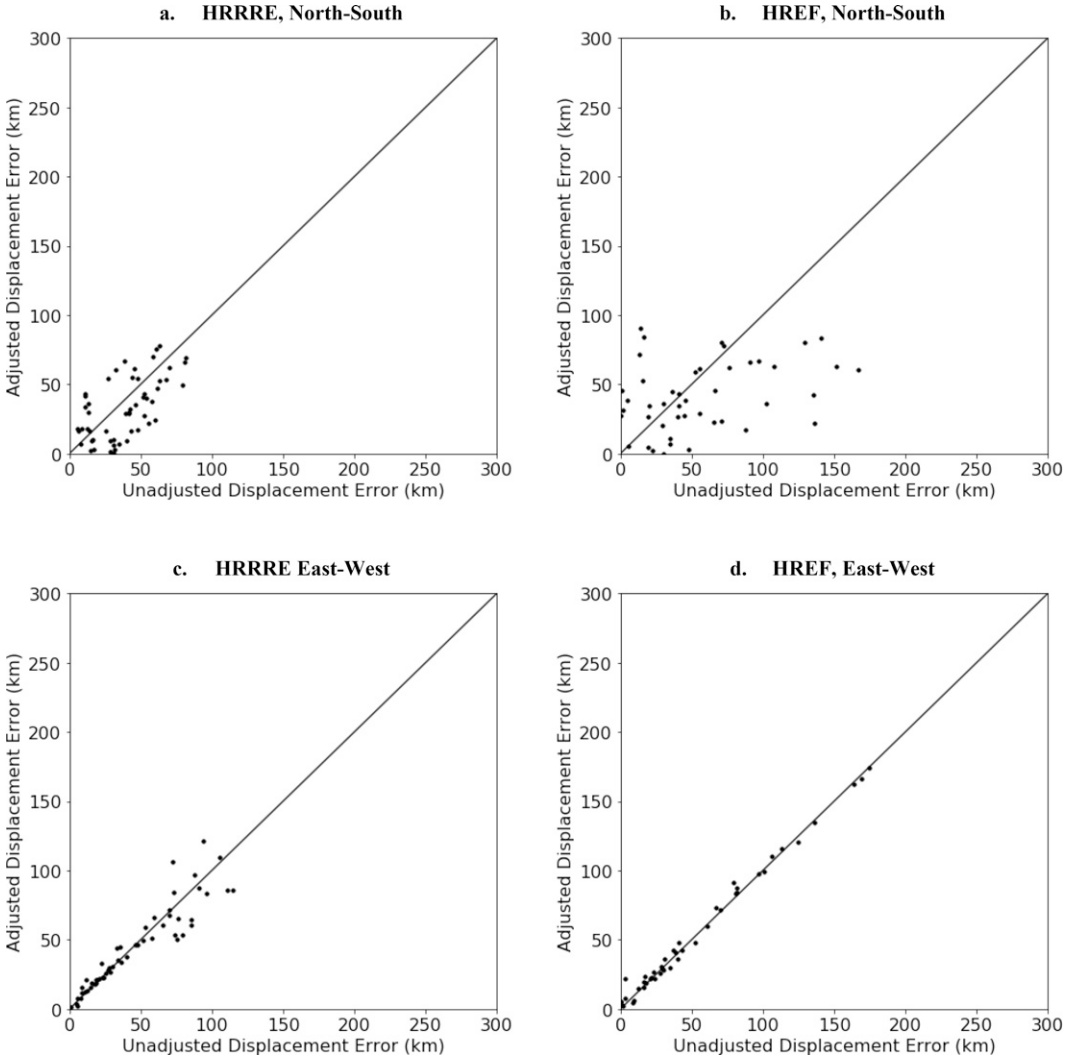

FIG. 14. As in Fig. 11, but for cases where the initiation hour displacement was in the SE quadrant.

TABLE 7. Mean reduction in displacement error and p values for the north–south (N–S) and east–west (E–W) components of displacement when the 0–18-h QPF centroid locations were adjusted using the ratios in Table 3. A negative mean reduction indicates that error increased instead of decreased. A p value greater than 0.95 (boldface) and 0.90 (italicized) indicates a confidence interval where the reduction in displacement error was statistically significant.

Quadrant of displacement at precipitation initiation	Mean error reduction for N–S displacement (km)	N–S p value	Mean error reduction for E–W displacement (km)	E–W p value
HRRRE				
NW	**13.32**	**0.992**	5.04	0.505
NE	**10.58**	**0.994**	8.84	0.874
SW	1.39	0.81	**7.12**	**0.965**
SE	**5.65**	**0.965**	−1.22	0.554
HREF				
NW	2.59	0.538	3.16	0.697
NE	*4.00*	*0.938*	**2.90**	**0.962**
SW	**0.57**	**0.952**	−1.96	0.381
SE	**14.96**	**0.976**	0.16	0.204

of rainfall intensity, areal coverage, complexity of rainfall pattern, and orientation of the rainfall footprint.

Acknowledgments. The authors thank Brett Roberts and the National Severe Storms Laboratory for granting access to HREF QPF data, and Bradley Carlberg for playing a pivotal role in initiating the research. The anonymous comments of three reviewers helped to improve the paper. This work was funded by the Iowa State University College of Liberal Arts and Sciences Dean's High Impact Award. Funding was also provided by NOAA CSTAR Grant NA17NWS4680005.

Data availability statement. All of the original HREF and HRRRE output used in this study are archived locally at Iowa State and not publicly accessible but are available upon request by contacting the corresponding author.

REFERENCES

Adams, T. E., and R. Dymond, 2019a: Possible hydrologic forecasting improvements resulting from advancements in precipitation estimation and forecasting for a real-time flood forecast system in the Ohio River Valley, USA. *J. Hydrol.*, **579**, 124138, https://doi.org/10.1016/j.jhydrol.2019.124138.

——, and ——, 2019b: The effect of QPF on real-time deterministic hydrologic forecast uncertainty. *J. Hydrometeor.*, **20**, 1687–1705, https://doi.org/10.1175/JHM-D-18-0202.1.

Aligo, E., B. Ferrier, and J. R. Carley, 2018: Modified NAM microphysics for forecasts of deep convective storms. *Mon. Wea. Rev.*, **146**, 4115–4153, https://doi.org/10.1175/MWR-D-17-0277.1.

Benjamin, S. G., and Coauthors, 2016: A North American hourly assimilation and model forecast cycle: The Rapid Refresh. *Mon. Wea. Rev.*, **144**, 1669–1694, https://doi.org/10.1175/MWR-D-15-0242.1.

Berner, J., S.-Y. Ha, J. P. Hacker, A. Fournier, and C. Snyder, 2011: Model uncertainty in a mesoscale ensemble prediction system: Stochastic versus multiphysics representations. *Mon. Wea. Rev.*, **139**, 1972–1995, https://doi.org/10.1175/2010MWR3595.1.

——, K. R. Fossell, S.-Y. Ha, J. P. Hacker, and C. Snyder, 2015: Increasing the skill of probabilistic forecasts: Understanding performance improvements from model-error representations. *Mon. Wea. Rev.*, **143**, 1295–1320, https://doi.org/10.1175/MWR-D-14-00091.1.

Carlberg, B., K. Franz, and W. Gallus Jr., 2020: A method to account for QPF spatial displacement errors in short-term ensemble streamflow forecasting. *Water*, **12**, 3505, https://doi.org/10.3390/w12123505.

Clark, A. J., W. A. Gallus Jr, M. Xue, and F. Kong, 2009: A comparison of precipitation forecast skill between small convection-allowing and large convective-parameterizing ensembles. *Wea. Forecasting*, **24**, 1121–1140, https://doi.org/10.1175/2009WAF2222222.1.

——, M. C. Coniglio, B. E. Coffer, G. Thompson, M. Xue, and F. Kong, 2015: Sensitivity of 24-h forecast dryline position and structure to boundary layer parameterizations in convection-allowing WRF model simulations. *Wea. Forecasting*, **30**, 613–638, https://doi.org/10.1175/WAF-D-14-00078.1.

——, and Coauthors, 2018: The Community Leveraged Unified Ensemble (CLUE) in the 2016 NOAA/Hazardous Weather Testbed Spring Forecasting Experiment. *Bull. Amer. Meteor. Soc.*, **99**, 1433–1448, https://doi.org/10.1175/BAMS-D-16-0309.1.

Coffer, B. E., L. C. Maudlin, P. G. Veals, and A. J. Clark, 2013: Dryline position errors in experimental convection-allowing NSSL-WRF model forecasts and the operational NAM. *Wea. Forecasting*, **28**, 746–761, https://doi.org/10.1175/WAF-D-12-00092.1.

Davis, C. A., B. Brown, and R. Bullock, 2006: Object-based verification of precipitation forecasts. Part I: Methodology and application to mesoscale rain areas. *Mon. Wea. Rev.*, **134**, 1772–1784, https://doi.org/10.1175/MWR3145.1.

Dowell, D. C., C. R. Alexander, T. Alcott, and T. Landwig, 2018: HRRR Ensemble (HRRRE) guidance 2018 HWT spring experiment. ESRL/GSD, 6 pp., https://rapidrefresh.noaa.gov/internal/pdfs/2018_Spring_Experiment_HRRRE_Documentation.pdf.

Gallus, W. A., 2012: The challenge of warm-season convective precipitation forecasting. *Rainfall Forecasting*, Nova Science Publishers, 129–160.

Gallus, W. A., Jr., J. Wolff, J. Halley Gotway, M. Harrod, L. Blank, and J. Beck, 2019: The impacts of using mixed physics in the Community Leveraged Unified Ensemble. *Wea. Forecasting*, **34**, 849–867, https://doi.org/10.1175/WAF-D-18-0197.1.

Hacker, J. P., and Coauthors, 2011: The U.S. Air Force Weather Agency's mesoscale ensemble: Scientific description and performance results. *Tellus*, **63A**, 625–641, https://doi.org/10.1111/j.1600-0870.2010.00497.x.

Hapuarachchi, H. A. P., Q. J. Wang, and T. C. Pagano, 2011: A review of advances in flash flood forecasting. *Hydrol. Processes*, **25**, 2771–2784, https://doi.org/10.1002/hyp.8040.

Hardy, J., J. J. Gourley, P.-E. Kirstetter, Y. Hong, F. Kong, and Z. L. Flamig, 2016: A method for probabilistic flash flood forecasting. *J. Hydrol.*, **541**, 480–494, https://doi.org/10.1016/j.jhydrol.2016.04.007.

Herman, G. R., and R. S. Schumacher, 2016: Extreme precipitation in models, an evaluation. *Wea. Forecasting*, **31**, 1853–1879, https://doi.org/10.1175/WAF-D-16-0093.1.

Hong, S.-Y., J. Dudhia, and S.-U. Chen, 2004: A revised approach to ice microphysical processes for the bulk parameterization of clouds and precipitation. *Mon. Wea. Rev.*, **132**, 103–120, https://doi.org/10.1175/1520-0493(2004)132<0103:ARATIM>2.0.CO;2.

——, Y. Noh, and J. Dudhia, 2006: A new vertical diffusion package with an explicit treatment of entrainment processes. *Mon. Wea. Rev.*, **134**, 2318–2341, https://doi.org/10.1175/MWR3199.1.

Janjić, Z. I., 1990: The step-mountain coordinate: Physical package. *Mon. Wea. Rev.*, **118**, 1429–1443, https://doi.org/10.1175/1520-0493(1990)118<1429:TSMCPP>2.0.CO;2.

Jankov, I., and W. A. Gallus Jr., 2004: MCS rainfall forecast accuracy as a function of large-scale forcing. *Wea. Forecasting*, **19**, 428–439, https://doi.org/10.1175/1520-0434(2004)019<0428:MRFAAA>2.0.CO;2.

Jirak, I. L., A. J. Clark, B. Roberts, B. Gallo, and S. J. Weiss, 2018: Exploring the optimal configuration of the High-Resolution Ensemble Forecast System. *25th Conf. on Numerical Weather Prediction*, Denver, CO, Amer. Meteor. Soc., 14B.6. https://ams.confex.com/ams/29WAF25NWP/webprogram/Paper345640.html.

Knebl Lowrey, M. R., and Z.-L. Yang, 2008: Assessing the capability of a regional-scale weather model to simulate extreme precipitation patterns and flooding in central Texas. *Wea.*

Forecasting, **23**, 1102–1126, https://doi.org/10.1175/2008WAF2006082.1.

Nakanishi, M., and H. Niino, 2009: Development of an improved turbulence closure model for the atmospheric boundary layer. *J. Meteor. Soc. Japan*, **87**, 895–912, https://doi.org/10.2151/jmsj.87.895.

Nielsen, E. R., and R. S. Schumacher, 2016: Using convection-allowing ensembles to understand the predictability of an extreme rainfall event. *Mon. Wea. Rev.*, **144**, 3651–3676, https://doi.org/10.1175/MWR-D-16-0083.1.

Rezacova, D., Z. Sokol, and P. Pesice, 2007: A radar-based verification of precipitation forecast for local convective storms. *J. Atmos. Res.*, **83**, 211–224, https://doi.org/10.1016/j.atmosres.2005.08.011.

Seo, D.-J., and J. P. Breidenbach, 2002: Real-time correction of spatially nonuniform bias in radar rainfall data using rain gauge measurements. *J. Hydrometeor.*, **3**, 93–111, https://doi.org/10.1175/1525-7541(2002)003<0093:RTCOSN>2.0.CO;2.

Seo, B.-C., F. Quintero, and W. F. Krajewski, 2018: High-resolution QPF uncertainty and its implications for flood prediction: A case study for the eastern Iowa flood of 2016. *J. Hydrometeor.*, **19**, 1289–1304, https://doi.org/10.1175/JHM-D-18-0046.1.

Squitieri, B. J., and W. A. Gallus Jr., 2016: WRF forecasts of Great Plains nocturnal low-level jet-driven MCSs. Part I: Correlation between low-level jet forecast accuracy and MCS precipitation forecast skill. *Wea. Forecasting*, **31**, 1301–1323, https://doi.org/10.1175/WAF-D-15-0151.1.

Stensrud, D. J., J. Bao, and T. T. Warner, 2000: Using initial condition and model physics perturbations in short-range ensemble simulations of mesoscale convective systems. *Mon. Wea. Rev.*, **128**, 2077–2107, https://doi.org/10.1175/1520-0493(2000)128<2077:UICAMP>2.0.CO;2.

Storm Prediction Center, 2019: Update history for SPC HREF ensemble viewer. NOAA Storm Prediction Center, https://www.spc.noaa.gov/exper/href/documentation/changelog.php.

Sukovich, E. M., F. M. Ralph, F. E. Barthold, D. W. Reynolds, and D. R. Novak, 2014: Extreme quantitative precipitation forecast performance at the Weather Prediction Center from 2001 to 2011. *Wea. Forecasting*, **29**, 894–911, https://doi.org/10.1175/WAF-D-13-00061.1.

Thompson, G., and T. Eidhammer, 2014: A study of aerosol impacts on clouds and precipitation development in a large winter cyclone. *J. Atmos. Sci.*, **71**, 3636–3658, https://doi.org/10.1175/JAS-D-13-0305.1.

Xuan, Y., I. D. Cluckie, and Y. Wang, 2009: Uncertainty analysis of hydrological ensemble forecasts in a distributed model utilising short-range rainfall prediction. *Hydrol. Earth Syst. Sci.*, **13**, 293–303, https://doi.org/10.5194/hess-13-293-2009.